CHEMISTRY
A EUROPEAN JOURNAL

DOI: 10.1002/chem.200501519

Theoretical Study of the Full Reaction Mechanism of Human Soluble Epoxide Hydrolase

Kathrin H. Hopmann and Fahmi Himo*[a]

Abstract: The complete reaction mechanism of soluble epoxide hydrolase (sEH) has been investigated by using the B3LYP density functional theory method. Epoxide hydrolases catalyze the conversion of epoxides to their corresponding vicinal diols. In our theoretical study, the sEH active site is represented by quantum-chemical models that are based on the X-ray crystal structure of human soluble epoxide hydrolase. The *trans*-substituted epoxide (1*S*,2*S*)-β-methylstyrene oxide has been used as a substrate in the theoretical investigation of the sEH reaction mechanism. Both the alkylation and the hydrolytic half-reactions have been studied in detail. We present the energetics of the reaction mechanism as well as the optimized intermediates and transition-state structures. Full potential energy curves for the reactions involving nucleophilic attack at either the benzylic or the homo-benzylic carbon atom of (1*S*,2*S*)-β-methylstyrene oxide have been computed. The regioselectivity of epoxide opening has been addressed for the two substrates (1*S*,2*S*)-β-methylstyrene oxide and (*S*)-styrene oxide.

Keywords: density functional calculations · enzyme catalysis · epoxide hydrolase · reaction mechanisms · regioselectivity

Introduction

Epoxides exhibit high chemical reactivity and biological organisms have therefore devised different strategies for converting epoxides into less reactive compounds. Epoxide hydrolases (EHs) catalyze the hydrolysis of epoxides to the corresponding vicinal diols (Scheme 1). In mammals, at least five different EHs have been recognized. These are the cholesterol epoxide hydrolase, the hepoxilin hydrolase, the leukotriene A_4 hydrolase, the soluble epoxide hydrolase, and the microsomal epoxide hydrolase.[1] Two of these, the soluble epoxide hydrolase (sEH) and the microsomal epoxide hydrolase (mEH), share large mechanistic similarities.[2–7] While mEH is located in the membrane of the endoplasmic reticulum, sEH is mainly found in cytosolic fractions. Both enzymes have broad substrate specificity and are involved in the detoxification of xenobiotic compounds, but also endogenous epoxides arising from lipid metabolism are among the substrates.[1,8] Based on structural data and sequence similarities with other enzymes, sEH and mEH are classified as members of the α/β-hydrolase fold superfamily.[9,10] Homologues of sEH and mEH are found in various organisms such as bacteria,[5] plants,[11,12] fungi,[13,14] and insects.[15] The different epoxide hydrolases seem to share a common mechanism but exhibit different substrate specificities, regio- and enantioselectivities, which makes them useful as biocatalysts for kinetic resolution and enantioconvergent conversion of a variety of epoxides.[16,17]

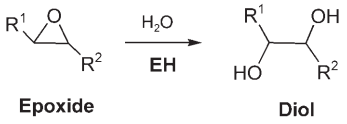

Scheme 1. Hydrolysis reaction catalyzed by epoxide hydrolases (EHs).

Initially, the reaction mechanism of EHs belonging to the α/β-hydrolase fold family was thought to proceed through a general base-catalyzed mechanism involving direct attack of an activated water molecule on the epoxide. However, sequence similarities with the bacterial haloalkane dehalogenases lead to the prediction that hydrolysis occurs through the formation of a covalent enzyme–substrate intermedi-

[a] K. H. Hopmann, Prof. Dr. F. Himo
Department of Theoretical Chemistry, School of Biotechnology
Royal Institute of Technology, Albanova University Center
SE-106 91 Stockholm (Sweden)
Fax: (+46) 8-5537-8590
E-mail: himo@theochem.kth.se

Supporting information (a brief discussion of a possible water-mediated proton shuttle between Tyr465 and Asp333, optimized geometries for attack at C2 of MSO, optimized geometries for regioselectivity studies with MSO in reversed orientation) for this article is available on the WWW under http://www.chemeurj.org/ or from the author.

ate.[10,18] The occurrence of this intermediate has indeed been verified for both sEH and mEH.[19–22] Mutational studies confirmed the presence of an Asp/Glu-His-Asp catalytic triad, similar to the one found in haloalkane dehalogenases.[2–7] A widely accepted version of the mechanism of sEH is shown in Scheme 2 (based on references cited in the text). In the first step of the reaction, the aspartate residue of the triad is suggested to perform a nucleophilic attack on the substrate, resulting in epoxide opening and formation of a covalent enzyme–substrate intermediate. This step is referred to as the alkylation half-reaction (Scheme 2, step A).[2–5,19] In the second step of the reaction, the hydrolytic half-reaction, the histidine residue acts as a general base, activating a water molecule which attacks the ester bond between the nucleophilic aspartate and the substrate (Scheme 2, step B).[3–7] The Asp/Glu-His residues of the catalytic triad form a charge-relay pair similar to the one known from serine proteases.[23] The tetrahedral intermediate thus formed dissociates to give the diol product (Scheme 2, step C). After product release, a new substrate can be bound (Scheme 2, step D). It is not clear when and how Tyr465 and the nucleophilic Asp333 are regenerated for the next catalytic cycle.

Four crystal structures of EHs belonging to the α/β-hydrolase fold family are known. These are the structures of the EH from *Agrobacterium radiobacter* AD1,[24] mouse sEH,[25,26] *Aspergillus niger* EH,[14] and human sEH.[27] All the structures show the proposed catalytic residues in similar positions. Additionally, all the structures determined exhibit two tyrosines in the active site which seem to have a perfect orientation for substrate binding and stabilization (Tyr465 and Tyr381 in human sEH, Scheme 2).[14,24–27] Mutagenesis studies support the role of the two tyrosines as possible hydrogen-bond/proton donors to the substrate.[28,29]

A conserved HG*X*P motif found in both mEH and sEH has also been implicated in the reaction mechanism (*X*= any residue).[10] This motif is involved in the formation of what is known as the oxyanion hole, which is also found in other enzymes belonging to the α/β-hydrolase fold family such as the haloalkane dehalogenases.[10,30] The oxyanion

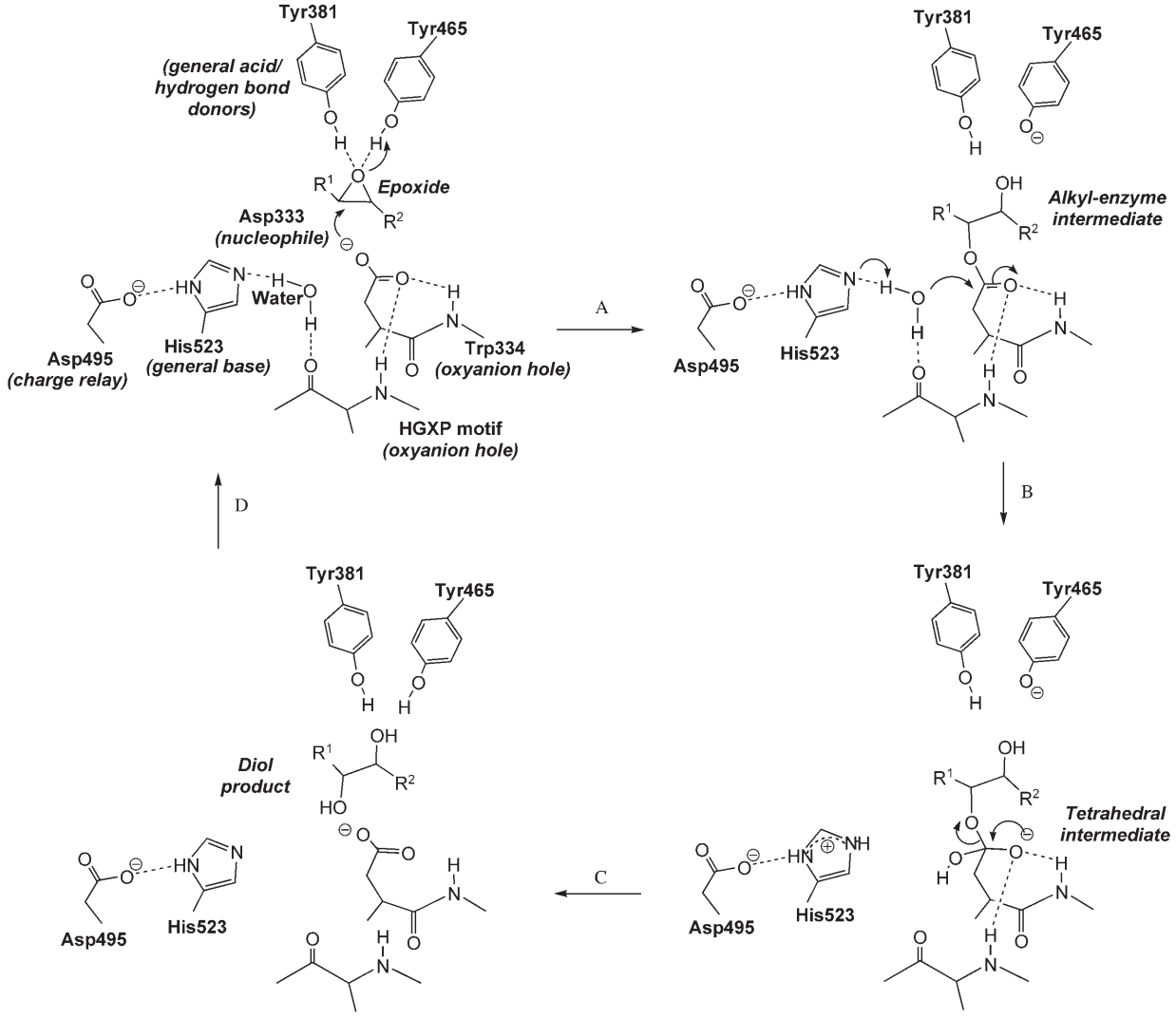

Scheme 2. Proposed sEH mechanism (residue numbering as in human sEH).

hole stabilizes the negative charge that evolves on the nucleophilic aspartate during hydrolysis of the covalent enzyme–substrate intermediate. The stabilization occurs through hydrogen bonding between the oxyanion and two backbone nitrogen atoms, one of which belongs to the *X* residue of the HG*X*P motif, while the other belongs to the residue that follows the nucleophilic aspartate (Scheme 2).[10,22]

Two theoretical studies have previously addressed part of the reaction mechanism of soluble epoxide hydrolases. In a small quantum-chemical approach, attack of acetic acid (as a model of the nucleophilic aspartate) on an epoxide in the presence or absence of an acid catalyst (a phenol, as a model of a tyrosine residue) was investigated.[31] It was concluded that acid catalysis lowers the activation barrier for alkylation significantly.[31] In a second theoretical study, molecular dynamics (MD) simulations were performed on murine sEH.[32] The study focused on the formation of near attack conformations (NACs) during the alkylation step. It was concluded that a hydrogen bond between the catalytic histidine and the nucleophilic aspartate might be necessary to keep the latter in a catalytically favorable position. The tyrosine residues were also suggested to have a role in determining the regioselectivity of epoxide opening.[32]

In the present study, we have used quantum-chemical models to investigate the reaction mechanism of soluble epoxide hydrolase in detail, including both the alkylation and the hydrolytic half-reactions. The quantum-chemical model is based on the X-ray crystal structure of human soluble epoxide hydrolase.[27] We present potential energy curves for the reaction and a detailed description of the transition states and intermediates involved. Additionally, the regioselectivity of epoxide opening is addressed for different substrates.

Computational Details

All the calculations presented here were performed using the B3LYP density functional theory method[33] as implemented in the Gaussian03 program package.[34] The calculations were performed in four steps. First, geometries were optimized with a medium-sized basis set. Next, the energies of the optimized geometries were evaluated with a much larger basis set. In the third step, the effects of the surrounding protein were estimated by using continuous dielectric medium techniques. In the fourth step, zero-point vibrational (ZPV) effects were evaluated by performing frequency calculations on the optimized geometries. The energies obtained from the large basis set calculations, corrected for solvation and ZPV effects, constitute the final energies.

The geometry optimizations were performed with the double-ξ plus polarization basis set 6-31G(d,p). In the optimizations, certain atoms of the models were fixed in their crystallographically observed positions (see Table 1). Single-point calculations on the optimized geometries were performed at the B3LYP/6-311+G(2d,2p) level of theory to obtain more accurate energies. The conductor-like polarizable continuum model[35] (CPCM) was employed at the B3LYP/6-31G(d,p) level of theory to obtain solvent effects. In this model, the solvent is represented by a homogeneous dielectric medium surrounding a cavity containing the solute. Single point calculations on the optimized structures were performed using a dielectric constant of $\varepsilon=4$, which is the standard value used in modeling protein surroundings. ZPV effects were computed by performing frequency calculations on the optimized geometries with the 6-31G(d,p) basis set. Frequency calculations were also used to confirm the nature of the various stationary points. The latter implies only positive eigenvalues for minima and one negative eigenvalue (imaginary frequency) for transition states. Fixing some atoms in their crystallographically observed positions gives rise to a few small negative eigenvalues for the optimized structures. These are, however, very small, in the order of -10 to $-20\ \mathrm{cm}^{-1}$, and do not affect the obtained results.

Quantum-chemical model: The model used in these calculations is based upon the crystal structure of human sEH complexed with the inhibitor *N*-cyclohexyl-*N*′-(iodophenyl)urea (CIU) (PDB code 1VJ5, Figure 1).[27] Parts of all the residues proposed to be catalytically important are included in the model, that is, Asp333, His523, Asp495, Tyr465, and Tyr381. Additionally, parts of the hydrogen-bond donors that constitute the oxyanion hole are included (Phe265 and Trp334) and also a crystallographically observed water molecule. In the human sEH crystal structure, this water molecule is found at a hydrogen-bonding distance of 2.78 Å from His523 (Figure 1). We therefore assumed that this water could be the catalytically active water molecule. Note that a water molecule in a similar position is observed in the crystal structures of the *A. radiobacter* AD1 and the *A. niger* EHs.[14,24] To model the catalytic reaction, the CIU inhibitor was manually replaced with a substrate. The epoxide chosen was the *trans*-substituted epoxide (1*S*,2*S*)-β-methylstyrene oxide (MSO). *trans*-Substituted epoxides are known to be good substrates of sEHs.[1,36] Experimentally, MSO has been shown to be a substrate of a variety of EHs, including human sEH, different rodent sEHs, and plant and fungi EHs.[36] Note that the MSO substrate was also used in MD simulations of mouse sEH.[32] In the human sEH crystal structure, the oxygen atom of the CIU

Table 1. Detailed description of the parts included in the human sEH active-site model.

	Part included from crystal structure	Proposed function/role in model	Fixed at position[a]
Asp333	whole side chain and part of backbone (Cα and C′)	nucleophilic attack on the substrate	Cα
His523	imidazole ring	general base; activates a water molecule	Cγ
Asp495	carboxylate (modeled as formic acid)	charge relay	H (former Cβ)
Tyr465	phenol	hydrogen bond/proton donor to epoxide	Cγ
Tyr381	phenol	hydrogen bond/proton donor to epoxide	Cγ
H_2O	water	hydrolyzes alkyl-enzyme intermediate	–
Phe265	part of backbone (N, Cα, and C′)	part of HG*X*P motif; stabilizes oxyanion formed on Asp333	backbone C′
Gly264	part of backbone (C′)	part of HG*X*P motif; included as extension to Phe265	backbone C′
Trp334	part of backbone (N and Cα)	stabilizes oxyanion formed on Asp333	Cα
Val497	part of side chain (Cβ and Cγ)	limits the flexibility of the substrate in the model	Cβ
Substrate MSO, SSO	phenyl ring and oxygen from CIU inhibitor; rest added manually	undergoes hydrolysis	–

[a] These atoms were kept fixed in their crystallographically observed positions during geometry optimizations.

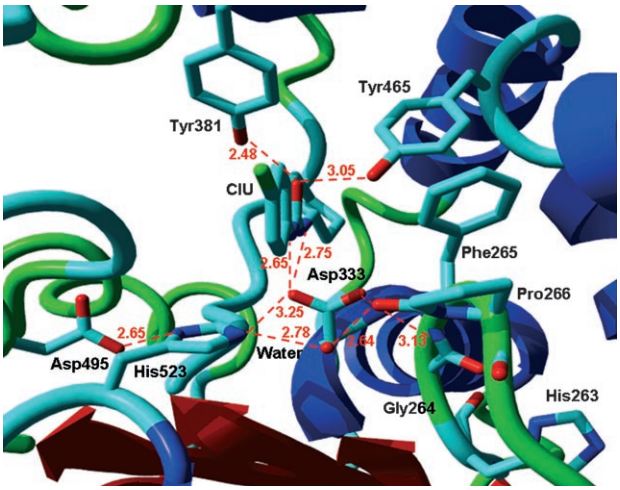

Figure 1. The human sEH active site with important residues shown in stick representation [this figure was prepared with YASARA (www.yasara.org) and PovRay (www.povray.org)]. Distances are in Å.

inhibitor is found to be within hydrogen-bonding distance of the two tyrosines, Tyr381 and Tyr465 (Figure 1). We assumed that the substrate would have the epoxide oxygen positioned similarly (see Scheme 2). In the chemical model, the CIU inhibitor was replaced with MSO by retaining the phenyl ring and oxygen atom of CIU and by adding the missing parts of MSO manually (see Scheme 3 for a comparison of the two compounds). The final quantum chemical model with MSO as substrate is composed of 98 atoms and has an overall charge of −2. The different parts of the model, their potential role, and points of truncation are summarized in Table 1. Additional calculations using (*S*)-styrene oxide (SSO) as substrate were performed to explore the regioselectivity of sEH. In these studies, SSO was constructed by replacing the methyl group at the C2 position of MSO with a hydrogen atom.

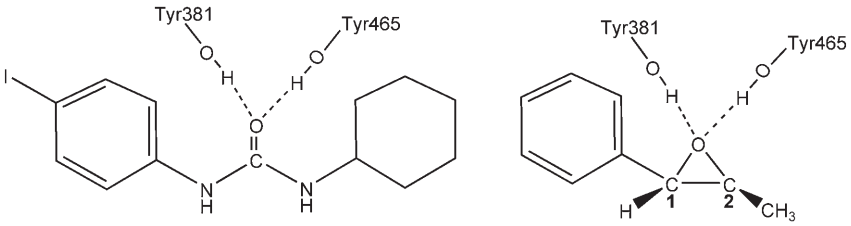

***N*-cyclohexyl-*N*′-(iodophenyl)urea (CIU)** **(1*S*,2*S*)-ß-methylstyrene oxide (MSO)**

Scheme 3. The CIU inhibitor found in the human sEH crystal structure (PDB 1VJ5).[27] In the chemical model, CIU was replaced with the substrate MSO.

Results and Discussion

Human-sEH-mediated hydrolysis of MSO: The optimized reactant species including the MSO substrate is shown in Figure 2A. The scheme next to the optimized geometries gives detailed information about the structure and the optimized distances. It can be seen that the substrate in the reactant is found to be in a perfect position for nucleophilic attack by Asp333. The distances from Asp333-Oδ2 to C1 and C2 of the substrate are 2.86 and 3.11 Å, respectively (in the following, Oδ2 refers to the Asp333 oxygen atom that performs the nucleophilic attack on the substrate, while Oδ1 is the Asp333 oxygen atom that hydrogen bonds to the Trp334 backbone nitrogen atom, see Figure 2A). The two tyrosines, Tyr465 and Tyr381, form hydrogen bonds to the epoxide oxygen, with distances of 2.73 and 2.72 Å, respectively (hydrogen-bond distances will here always refer to the distance between the donor and acceptor atoms). A hydrogen bond is also observed between Asp495 and the Nδ atom of His523, with a distance of 2.73 Å. The Nδ–H bond of His523 is slightly elongated and has a length of 1.06 Å. The water molecule is hydrogen bonded to the Nε atom of His523 and to the Phe265 backbone carbonyl. Hydrogen bonds are also observed between the backbone nitrogen atoms of Phe265 and Trp334 and the Oδ1 atom of Asp333, with lengths of 2.75 and 2.97 Å, respectively. The two hydrogen bonds are of special interest as they constitute the oxyanion hole that stabilizes the negatively charged tetrahedral intermediate formed during the hydrolytic half-reaction.

The transition state (TS) for the nucleophilic attack of Asp333 at C1 of MSO was optimized and the associated barrier was found to be 7.8 kcal mol^{-1} (see Figure 4 for the full energy curve). The optimized TS geometry is seen in Figure 2B. Nucleophilic attack occurs at a distance of 2.29 Å between the epoxide C1 and Oδ2 atom of Asp333. In the TS, the oxirane ring is partially opened with an O–C1 distance of 1.89 Å. The distances between the epoxide oxygen and the phenol oxygen atoms of the two tyrosines are shortened to 2.61 and 2.64 Å for Tyr465 and Tyr381, respectively. Note that none of the tyrosine protons is transferred to the epoxide oxygen in the alkylation TS. Instead, protonation of the epoxide oxygen atom seems to occur in a distinct step, as described below.

The covalent enzyme–substrate intermediate (CI) formed during the alkylation step was optimized and found to have a relative energy of −8.0 kcal mol^{-1}. In the optimized CI structure, the epoxide oxygen atom is not protonated and forms hydrogen bonds to the two tyrosines with a length of 2.49 Å to Tyr465 and 2.51 Å to Tyr381 (Figure 2C). The O–H bonds of the two tyrosines are somewhat elongated to 1.06 Å for Tyr381 and 1.07 Å for Tyr465. Attempts were subsequently made to optimize a CI in which a proton has been transferred from one of the tyrosines to the epoxide oxygen atom. A stable geometry could only be optimized if the proton was transferred from Tyr465. The resulting protonated CI is shown in Figure 2D and is found at a relative energy of −8.6 kcal mol^{-1} below the reactant, that is, only 0.6 kcal mol^{-1} lower than the unprotonated CI. The TS for the proton transfer from Tyr465 to the epoxide oxygen atom was optimized and found to be very facile. In fact, the optimized TS is calculated to have a slightly negative barrier of

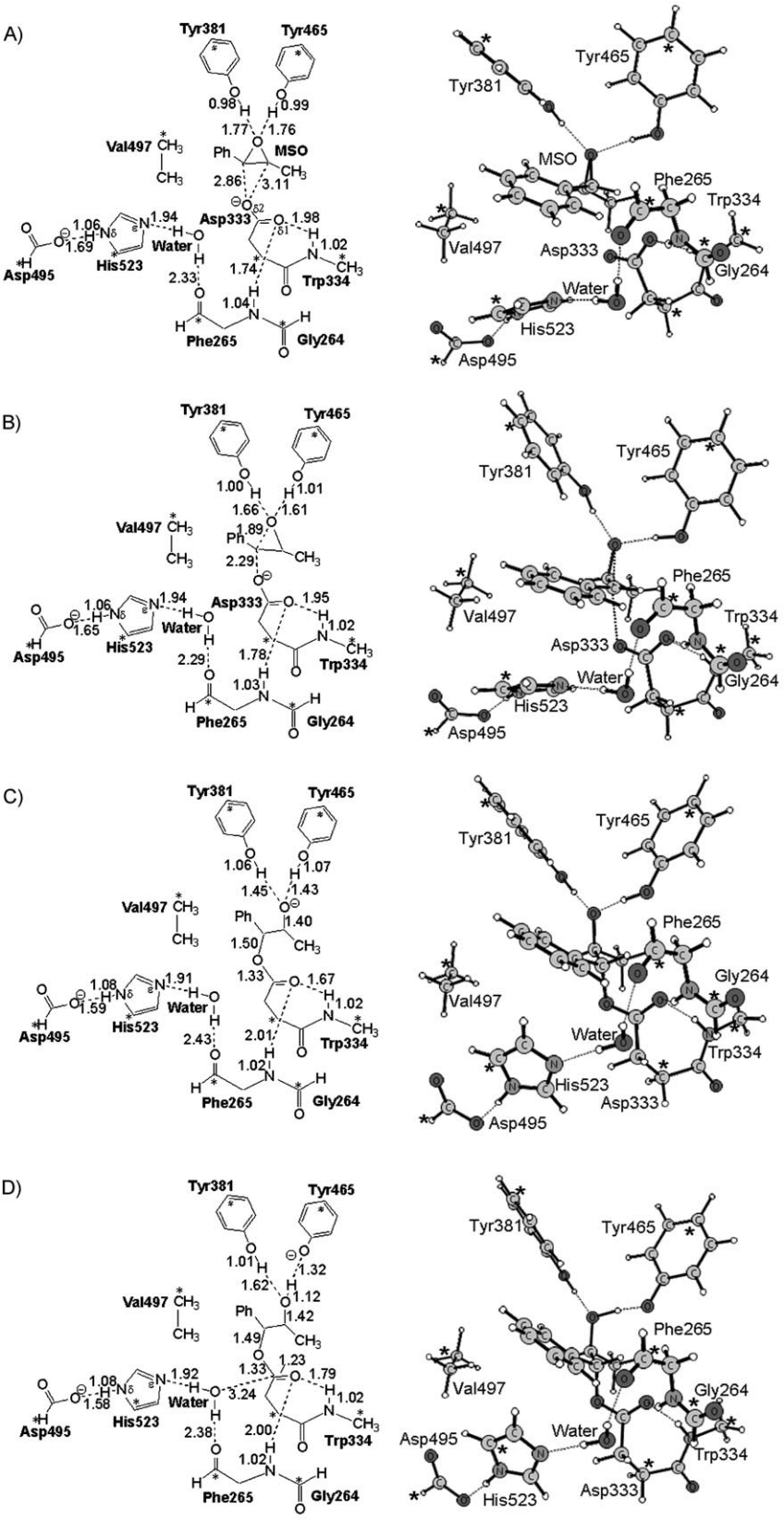

Figure 2. Optimized geometries for the alkylation half-reaction (attack at C1 of MSO). A) Reactant, B) alkylation TS, C) unprotonated covalent intermediate (CI), and D) CI protonated at the epoxide oxygen. The optimized geometries are shown on the right. Detailed information about the structures and the optimized distances (in Å) are shown in schemes on the left. Asterisks indicate the atoms fixed in their crystallographically observed positions in the calculations.

$-1.0\,\mathrm{kcal\,mol^{-1}}$, which should be viewed as an error of the methods used. DFT has been shown to underestimate barriers and if the reaction barrier is very low, reactions are sometimes predicted to be barrierless or even have a negative barrier.[37] This underestimation might be due to the inherent self-interaction error of DFT.[38,39] Another reason for the slightly negative barrier could be that the geometry is optimized with one basis set and the energy is evaluated with another much larger basis set (see Computational Details). The potential energy surfaces using the two different basis sets can sometimes be slightly shifted relative to each other, which might lead to an underestimation of barriers. Note that we also investigated whether the epoxide could be protonated prior to the nucleophilic attack by Asp333, but no stable intermediate could be optimized.

Following the formation of the covalent intermediate, the ester formed is proposed to be hydrolyzed by a water molecule, which is activated by His523 (Scheme 2). We have optimized the TS for the attack of water at the carbonyl carbon atom of Asp333 (Figure 3A). The associated barrier for the water attack TS is calculated to be $18.1\,\mathrm{kcal\,mol^{-1}}$ relative to the protonated CI. In the TS, His523 abstracts a proton from water, which performs a nucleophilic attack at the Asp333 carbonyl carbon atom. The distance between the carbonyl carbon and the water oxygen is 1.74 Å, while the water proton is found 1.23 Å from the water oxygen and 1.27 Å from the Nε atom of His523. His523-mediated activation of water is facilitated by the charge-relay residue Asp495, which in concert with

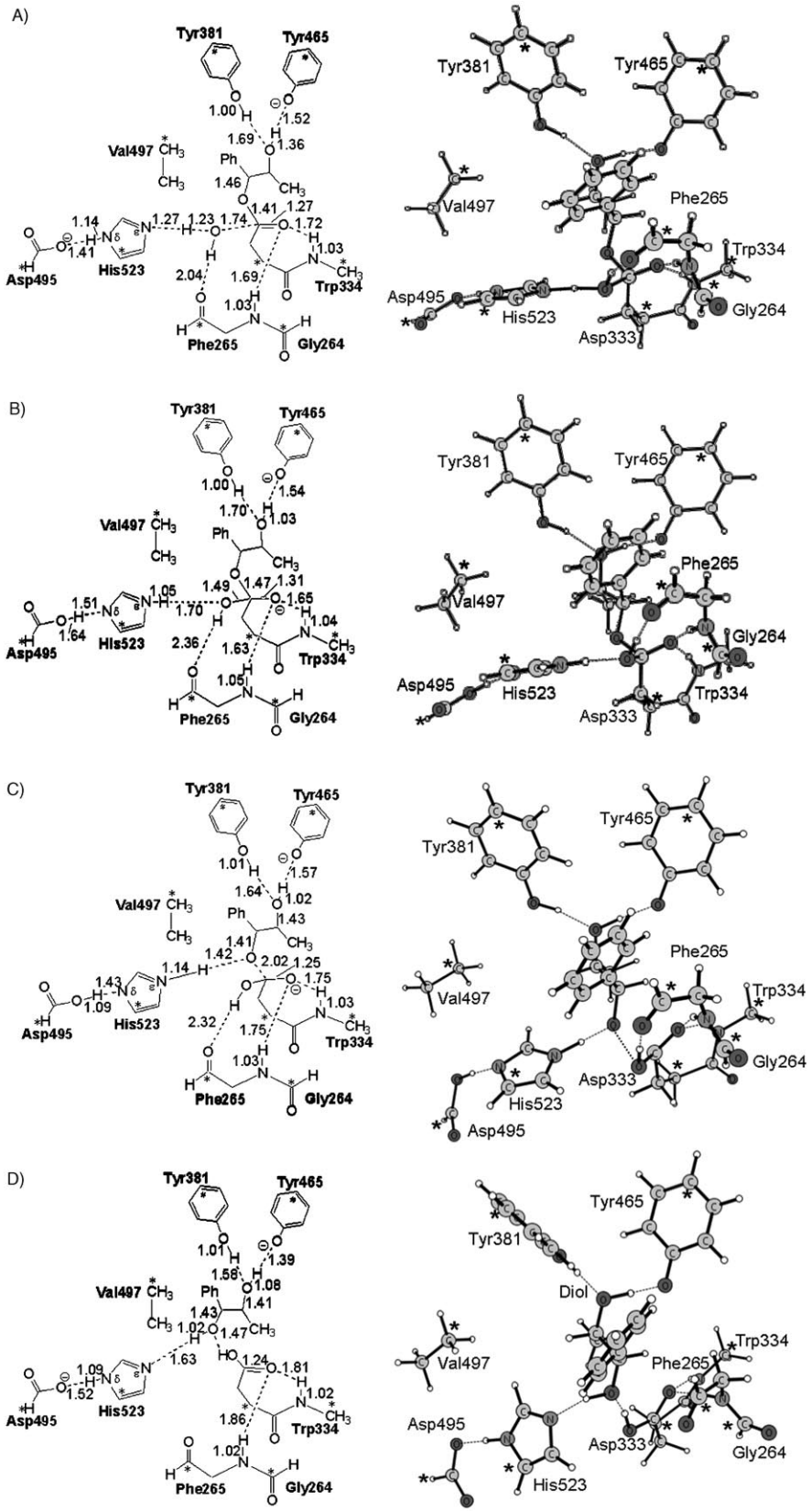

Figure 3. Optimized geometries for the hydrolytic half-reaction (attack at C1 of MSO). A) TS of water attack, B) tetrahedral intermediate, C) TS for dissociation of the tetrahedral intermediate, and D) product geometry of (1*R*,2*S*)-1-phenyl-1,2-propanediol.

water attack on the CI abstracts a proton from the Nδ atom of His523. The overall mechanism for this step can hence be referred to as a concerted double proton transfer (DPT) mechanism. It is possible, however, that the calculated DPT is an artefact of our model and that a single proton transfer (SPT) mechanism would be favored when employing a larger model. This is discussed in more detail below.

Attack of water at the carbonyl carbon of Asp333 results in the formation of a tetrahedral intermediate. The optimized structure is found to have an energy 1.0 kcal mol^{-1} below the TS for water attack, that is, 17.1 kcal mol^{-1} higher than the protonated CI. As proposed in Scheme 2, the tetrahedral intermediate is stabilized by hydrogen bonds from the Oδ1 atom of Asp333 to the backbone nitrogen atoms of Phe265 and Trp334 (Figure 3B). The hydrogen-bond length is 2.66 Å for the Phe265–Asp333 interaction and 2.68 Å for the Trp334–Asp333 interaction. Their lengths have thus been shortened relative to the protonated CI, for which the lengths are 2.89 and 2.78 Å, respectively.

To obtain the product, the C–O bond between the substrate and Asp333 has to be broken. Also, to obtain the final diol, the oxyanion formed on the product after bond dissociation has to be protonated. Possible proton sources are the two former water protons, one of which is now found on the Nε atom of His523. We investigated whether dissociation of the tetrahedral intermediate and protonation of the emerging oxyanion of the product occur in a stepwise or a concerted fashion. From our calculations we conclude that the two events occur concertedly.

The TS for the concerted bond dissociation and proton transfer from the Nε atom of His523 to the alcohol oxygen atom of the former Asp333 ester can be seen in Figure 3C. Cleavage of the C–O bond occurs at 2.02 Å, while the proton is found at a distance of 1.14 Å from the Nε atom of His523 and 1.42 Å from the emerging oxyanion of the diol product. The barrier for dissociation of the tetrahedral intermediate is 5.5 kcal mol^{-1} calculated relative to the tetrahedral intermediate, that is, 22.6 kcal mol^{-1} relative to the protonated CI. From Figure 4 it is thus evident that the hydrolytic half-reaction is the rate-determining step of the reaction.

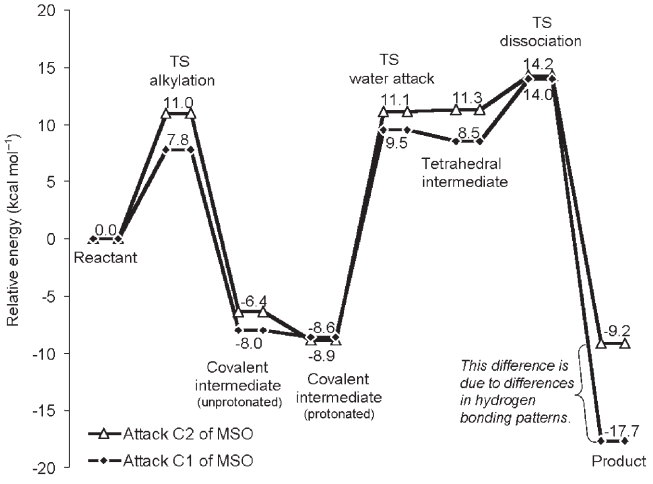

Figure 4. Computed energies for the hydrolysis of MSO by human sEH.

The structure of the final protonated (1*R*,2*S*)-1-phenyl-1,2-propanediol product was optimized and is shown in Figure 3D. It is found to have an energy of −17.7 kcal mol^{-1} relative to the reactant state. This is lower than the overall driving force for the reaction, which is calculated as the exothermicity of the reaction of the free substrate and H_2O and which is found to be −10.4 kcal mol^{-1} for MSO. Note that several different geometries of the final diol product could be optimized. They differ in the hydrogen-bonding pattern between the diol and the surrounding residues and exhibit significantly different energies. The structure shown in Figure 3D has a hydrogen-bonding pattern closest to that of the reactant state.

Note that in the product geometry shown in Figure 3D, Asp333 is protonated, while Tyr465 is deprotonated. To prepare the active site for a new catalytic cycle, both Tyr465 and Asp333 need to be regenerated and a new catalytic water molecule needs to be bound. We suggest that following product release, a water-mediated proton shuttle could transfer the proton from Asp333 to Tyr465, thereby regenerating both residues. We have tested the possibility of such a proton transfer and found an overall barrier of less than 2 kcal mol^{-1}. Further details about the possible water proton shuttle are given in the Supporting Information.

The results presented above confirm that the mechanism as shown in Scheme 2 is energetically feasible. The two tyrosines, Tyr465 and Tyr381, bind the substrate and position it for nucleophilic attack by Asp333. The covalent enzyme–substrate intermediate is protonated by Tyr465, which seems to occur in a distinct step. The covalent bond formed is hydrolyzed with aid from the Asp495-His523 unit, which first abstracts a proton from the catalytic water molecule and in the next step donates the proton to the emerging diol. The role of the oxyanion hole in stabilizing the tetrahedral intermediate is also confirmed by our calculations.

Regioselectivity of epoxide opening: Since epoxide opening can occur at two different carbon atoms, it is of interest to establish if a certain substrate is hydrolyzed in a regioselective manner. The regioselectivity of epoxide opening is usually governed by electronic and steric factors, both of which are determined by the substitution pattern at the two epoxide carbon atoms. If the epoxide has a primary (unsubstituted) carbon atom, attack is often preferred there due to the steric advantage. If one of the epoxide carbon atoms has a substituent capable of stabilizing the positive charge developed during epoxide opening, attack might be preferred at the substituted carbon atom. The electronic advantage for attack at the substituted carbon atom is enhanced in the presence of an acid catalyst.[40]

In addition to the results presented above for epoxide opening at the C1 atom, we have studied the full reaction mechanism for epoxide opening at the homo-benzylic position (C2) of MSO. The reaction proceeds through exactly the same steps as the attack at C1. The associated energies, however, are somewhat different (Figure 4). The regioselectivity of epoxide opening is determined in the alkylation step. The optimized TS for nucleophilic attack at the C2 atom is shown in Figure 5. The distance between C2 and the Oδ2 atom of Asp333 is 2.21 Å in the TS, slightly shorter

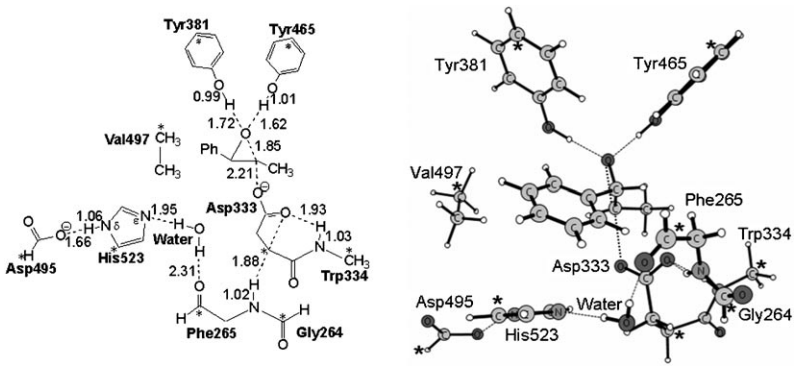

Figure 5. Optimized alkylation TS for attack at C2 of MSO.

than for the C1 atom (2.29 Å). The calculated barrier is 11.0 kcal mol^{-1}, which is 3.2 kcal mol^{-1} above the barrier calculated for attack at the C1 atom. The computed energies indicate that attack is preferred at the benzylic position of MSO. This could be expected from the properties of MSO. Both the epoxide carbon atoms of MSO are singly substituted (Scheme 3) and although the methyl group on C2 is smaller than the phenyl substituent on C1, it can be assumed that there is no or very little steric advantage for attack at C2. The regioselectivity of epoxide opening is thus governed by electronic factors only. In the alkylation TS, the epoxide ring is partially opened, resulting in the development of a positive charge on the carbon atom that is attacked by the nucleophile. The positive charge is better stabilized on the benzylic carbon (owing to the electronic properties of the phenyl substituent) and attack will hence be preferred there.

As noted above, problems with multiple minima start to arise with a model of this size. This is also a problem during the optimization of the covalent intermediate geometries for attack at C2 of MSO. For both the unprotonated and the protonated CIs formed by attack at C2 of MSO, different structures could be optimized which differ with respect to the hydrogen bond formed by the backbone nitrogen atom of Phe265. This hydrogen bond is either to the Oδ1 atom of Asp333 (Phe265-N–H···Oδ1-Asp333) or to the water oxygen atom (Phe265-N–H···OH_2). The Phe265-N–H···OH_2 structures are lower in energy than the Phe265-N–H···Oδ1-Asp333 structures, 1.8 kcal mol^{-1} for the unprotonated C2 CI and 0.3 kcal mol^{-1} for the protonated C2 CI. However, the Phe265-N–H···OH_2 structures are considered to belong to a different local minimum than the reactant in which the hydrogen bond is Phe265-N–H···Oδ1-Asp333. To be able to compare the relative energies, the same local minimum should be kept and care was thus taken to keep this part of the model in the same local minimum throughout the reaction. Unfortunately, optimization of the geometry of the product of attack at C2 of MSO, (1*S*,2*R*)-1-phenyl-1,2-propanediol, was not possible in the same local minimum as the preceding geometries. The C2 product could only be optimized in another minimum, in which the hydrogen bond between the Oδ1 atom of Asp333 and the Trp334 backbone nitrogen atom was lost. The hydrogen-bonding pattern of this geometry also differs in other aspects from the product geometry optimized for attack at C1 (the optimized geometries for attack at C2 of MSO are shown in Figure S2A—F of the Supporting Information). This explains the large difference in energy observed between the two products (Figure 4).

To further investigate the regioselectivity of epoxide opening, we also studied the opening of another substrate, (*S*)-styrene oxide (SSO). SSO is similar to MSO, but lacks the methyl group on C2. It is thus interesting to investigate if the steric advantage for attack at the terminal carbon atom (C2) of this substrate is sufficient to exceed the electronic advantage for attack at the benzylic position (C1). For SSO, only the geometries of the reactant and the alkylation transition states for attack at C1 and C2 were optimized (the geometries can be found in the Supporting Information, Figure S3A–C). The barrier for attack at the benzylic position of SSO was found to be 6.3 kcal mol^{-1}, while attack at the terminal carbon (C2) of SSO has a barrier of 7.0 kcal mol^{-1}. SSO thus still exhibits preferred attack at the benzylic position, albeit with a difference in barriers of only 0.7 kcal mol^{-1}. This indicates that hydrolysis of SSO should lead to a mixture of products. The small difference between the two barriers, however, suggests that the regioselectivity of SSO opening could be influenced by substrate binding in the active site. If SSO is bound in such a way that a small steric advantage for attack at either carbon is obtained, exclusive attack at that carbon might be observed.

As noted above, the positioning of the substrate in our model was based on the position of the CIU inhibitor in the human sEH crystal structure (PDB 1VJ5, Figure 1).[27] Interestingly, in the mouse sEH structure (PDB 1EK1),[26] the same inhibitor is bound in a reverse orientation, with the phenyl group in the place where the cyclohexyl ring is found in the human structure. This indicates that a given substrate might also be accommodated in a reverse orientation. We tested what effect such a reverse orientation, that is, rotation of the MSO substrate by approximately 180°, would have on the alkylation barrier as well as on the regioselectivity of epoxide opening. The optimized structure of the alkylation transition state for attack at C1 of MSO in the reversed orientation is shown in Figure 6 (optimized geometries of the reactant and the alkylation TS for attack at C2 of MSO in the reversed orientation can be found in the Supporting Information, Figure S4A,B). The barriers for the opening of MSO in the reversed orientation are 7.5 kcal mol^{-1} for attack at C1 and 11.1 kcal mol^{-1} for attack at C2. These values are almost identical to the barriers obtained with the original model, which are 7.8 and 11.0 kcal mol^{-1} for attack at C1 and C2, respectively. Reversing the orientation of the

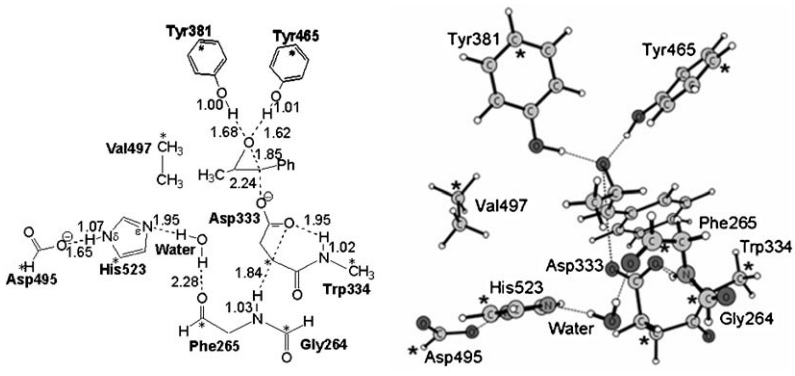

Figure 6. Optimized alkylation TS for attack at C1 of MSO in the reversed orientation.

substrate does thus not appear to have any significant effect on the alkylation barriers or on the regioselectivity of epoxide opening.

Comparison with experimental results: The kinetic mechanism of the epoxide hydrolases discussed here is generally described by Equation (1),[41] where E = enzyme, S = substrate, E·S = enzyme–substrate complex, E–S = covalent enzyme–substrate intermediate, P = product, K_s = binding constant, k_2 = alkylation rate, k_{-2} = dealkylation rate, and k_3 = the rate of the hydrolytic step. The enzyme–substrate complex formed upon binding of the substrate in the active site (also referred to as the Michaelis complex) corresponds to our reactant state. Experimentally, the product is usually formed in two kinetic steps from the Michaelis complex, alkylation and hydrolysis. The alkylation half-reaction has been found to be reversible and therefore both the alkylation (k_2) and dealkylation rates (k_{-2}) are of interest. The hydrolytic half-reaction, however, seems to be essentially irreversible and only the forward rate k_3 is considered.[41,42]

$$\mathrm{E+S} \underset{}{\overset{K_s}{\rightleftharpoons}} \mathrm{E{\bullet}S} \underset{k_{-2}\ (\textit{Dealkylation})}{\overset{k_2\ (\textit{Alkylation})}{\rightleftharpoons}} \mathrm{E\text{-}S} \xrightarrow{k_3\ (\textit{Hydrolysis})} \mathrm{E+P} \qquad (1)$$

A detailed study of the kinetics of MSO hydrolysis by human sEH has to our knowledge not been published. However, detailed kinetics have been reported for the hydrolysis of styrene oxide and *p*-nitrostyrene oxide by *A. radiobacter* AD1 EH,[28,42] the hydrolysis of glycidyl-4-nitrobenzoate by rat mEH,[41] and the hydrolysis of *trans*-stilbene oxide by potato EH (StEH1).[12] The kinetics of the hydrolysis of chalcone oxides by human and mouse sEHs has also been studied.[29,43] Although the substrates and enzymes differ from our study, some general conclusions can be drawn from the experimental results.

Experimental rate constants for the alkylation half-reaction (k_2) for *A. radiobacter* AD1 EH, rat mEH, and potato EH with the above substrates are found to be in the range of 100–1100 s^{-1}.[12,28,41,42] This can be converted to barriers of around 13–15 kcal mol^{-1} by using classical transition-state theory. The alkylation rates found for enzymatic reactions of mouse and human sEHs with the chalcone oxides are much lower, between 0.09 and 0.75 s^{-1}, corresponding to barriers of around 18–19 kcal mol^{-1}.[43] Chalcone oxides, however, are considered to be poor sEH substrates and their barriers are assumed to be higher than what would be expected for a good substrate.[29,43] We calculated a barrier of only 7.8 kcal mol^{-1} for Asp333-mediated nucleophilic attack at C1 of MSO. Comparison of this value with the experimentally observed rates indicates that the computed alkylation barrier might be underestimated. In this context note that the optimized product geometry (Figure 3D) indicates that the exothermicity of the enzymatic reaction is larger than the exothermicity of the reaction of the free substrate and H_2O, −17.7 versus −10.4 kcal mol^{-1}. From this it can be estimated that the release of the product and binding of a new substrate should cost around 7.3 kcal mol^{-1}. One can argue that this energy should be added to the first step of the next reaction cycle, in which case the alkylation barrier would increase from 7.8 to 15.1 kcal mol^{-1}, which is in much better agreement with the experimental rates discussed above.

In our calculations, we observe nucleophilic attack on the epoxide and protonation of the oxyanion formed as distinct steps. Protonation of the epoxide by one of the tyrosines is generally believed to occur in concert with nucleophilic attack, that is, through a push–pull mechanism.[26,28] It is possible that the lack of proton transfer in the alkylation TS is an artefact of our quantum chemical model. Inclusion of additional residues around the two tyrosines could affect the observed result. For example, it has been proposed that a Tyr465 tyrosinate is stabilized by edge-to-face interactions with the side-chains of the nearby Trp334 and Phe385 residues.[25,29] Inclusion of the Trp334 and Phe385 side-chains might aid deprotonation of Tyr465 and could thus result in a TS in which nucleophilic attack and proton transfer occur concertedly. However, since the quantum chemical model presented already is quite large, it was not possible to include further residues. Note also that very recent experimental data support a scenario in which protonation and alkylation do not occur concertedly. The amount of tyrosinate formed during the alkylation step of potato EH was measured to correspond to approximately 0.4 tyrosinates per enzyme molecule, indicating only partial ionization of one (or both) of the tyrosines.[44] Our theoretical results offer an explanation for this observation. The computed energy difference between the unprotonated and protonated covalent intermediates is small (0.6 kcal mol^{-1} for attack at C1 of MSO, Figure 4) and indicates that the two species will be in equilibrium, especially because the barrier for the following step, the hydrolytic half-reaction, is very high. There will thus be a mixture of protonated and unprotonated covalent intermediates present, which would explain the partial ionization observed experimentally. Interestingly, with our model, a stable protonated covalent intermediate could only be optimized if the proton was transferred from Tyr465. It is usually suggested that Tyr465 is the proton donor to the epoxide since analogs of Tyr465 are highly conserved in all α/β-hydrolase fold EHs, while Tyr381 only seems to be conserved in the soluble and not the microsomal EHs.[25] It is not clear why proton transfer from Tyr381 failed in our calculations since both Tyr381 and Tyr465 are modeled as phenols and thus should be equivalent.

As noted, the alkylation reaction has been shown to be reversible.[41,42] Experimentally, the alkylation rate is found to be significantly higher than the dealkylation rate for rat mEH and *A. radiobacter* AD1 EH, that is, $k_2 \gg k_{-2}$.[41,42] Depending on the substrate, k_2/k_{-2} is found to vary between 28 and 555 for rat mEH and *A. radiobacter* AD1 EH. This ratio suggests a stabilization of the CI relative to the reactant of 2–4 kcal mol^{-1}. Our computed value of 8.6 kcal mol^{-1}

therefore indicates an overstabilization of the CI in our computational model. One possible explanation for this calculated overstabilization could be the solvation model used. In the gas phase, the CI is calculated to lie 12.8 kcal mol^{-1} below the reactant. With solvation effects (homogeneous solvent with $\varepsilon = 4$) this value decreases to 8.6 kcal mol^{-1}. The observed decrease in stability of the CI indicates that inclusion of additional specific protein environment might result in a less stabilized CI and better agreement with the value expected from experiment. By the same reasoning as above, one can argue that if the 7.3 kcal mol^{-1} difference in binding between the product and the substrate is added to the reactant energy, the CI would be stabilized by only 1.3 kcal mol^{-1} (8.6–7.3 kcal mol^{-1}). This would result in a reversible reaction in better agreement with the experimental rates.

In our model, the attack of water on the alkyl-enzyme intermediate occurs through a concerted double proton transfer (DPT) mechanism, as described above (Figure 3A). A charge-relay mechanism similar to this is also found in serine proteases, although here it is a matter of debate whether the aspartate of the Asp-His pair actually abstracts a proton from HisNδ (corresponding to a DPT mechanism) or if the aspartate remains anionic and only provides electrostatic stabilization to the protonated histidine [corresponding to a single proton transfer (SPT) mechanism]. For the serine proteases, experimental and theoretical support for both the SPT and the DPT mechanisms can be found.[45] In a computational study of a model of the serine proteases, the SPT and DPT mechanisms were shown to have comparable energies.[46] It was pointed out, however, that if additional residues capable of stabilizing an anionic aspartate were to be included in the serine protease model, this might result in an energetically favored SPT mechanism.[46] Similarly, in our model of sEH, inclusion of a larger portion of the protein environment surrounding Asp95 might stabilize its anionic form and favor a SPT mechanism over the observed DPT mechanism. Several possible hydrogen-bonding donors to Asp495 are present in the sEH crystal structure, for example, the protein backbone of Val 497 and Leu498 and the amide side-chain of Asn357.

From our calculations, the hydrolytic half-reaction is found to be the rate-determining step of the mechanism. Consistently with this, the hydrolytic half-reaction has been shown to be rate-determining for *A. radiobacter* AD1 EH,[42] potato EH,[12] and rat mEH.[41] The overall barrier for the hydrolytic half-reaction is calculated to be 22.6 kcal mol^{-1} (for attack at C1) with our model. Experimental rate constants for the hydrolytic step (k_3) for *A. radiobacter* AD1 EH, rat mEH, and potato EH with the substrates mentioned above are found to be in the range of 0.07–24 s^{-1}, indicating hydrolysis barriers of 15.8–19 kcal mol^{-1}.[12,28,41,42] As noted above, we assume that the CI might be somewhat overstabilized in our calculations. Raising the CI by a few kcal mol^{-1} would reduce the barrier for the hydrolytic step and bring it closer to the experimentally observed barriers.

Finally, the theoretically determined regioselectivity shows preferred attack at the benzylic position (C1) of (1*S*,2*S*)-β-methylstyrene oxide (MSO). The calculated barrier for attack at C2 relative to C1 is 3.2 kcal mol^{-1} higher (3.6 kcal mol^{-1} in the reversed substrate orientation). Experimentally, it has been shown that attack at the benzylic carbon atom of MSO is indeed preferred if hydrolyzed by mouse sEH,[36] rabbit sEH,[47] or *Aspergillus terreus* EH.[48] The regioselectivity was reported to be 100, 98, and 95% for attack at the C1 atom of MSO for the three enzymes, respectively.[36] These regioselectivities are in good agreement with our theoretical result for human sEH, which indicate exclusive attack at the benzylic position of MSO. Note, however, that not all EHs display the same regioselectivity with this substrate. Experimentally, rabbit microsomal EH exhibits preferred attack at the homo-benzylic (C2) position of MSO.[47] For (*S*)-styrene oxide (SSO), we find a difference in barrier for attack at the benzylic position (C1) and the terminal position (C2) of only 0.7 kcal mol^{-1}. This small difference indicates the formation of a mixture of products. In agreement with this, rabbit-sEH-mediated hydrolysis of SSO leads to 45% attack at the benzylic position and 55% attack at the terminal position.[47] For the *A. radiobacter* AD1 EH, however, experiments show that attack occurs exclusively at the terminal carbon atom of SSO.[42,49] The catalytic residues of *A. radiobacter* AD1 EH and human sEH, including the two tyrosines, are identical, indicating that other differences in the active site account for the different regioselectivities.

Conclusion

In this paper, we have presented a detailed description of the reaction mechanism of human soluble epoxide hydrolase. Quantum chemical models were employed to optimize intermediates and transition states for the entire reaction mechanism, including both the alkylation and the hydrolytic half-reactions. The theoretical results for human-sEH-mediated hydrolysis of (1*S*,2*S*)-β-methylstyrene oxide (MSO) agree in important aspects with experimental results obtained for other epoxide hydrolases. Our results show that the reaction mechanism as shown in Scheme 2 is energetically feasible. The proposed roles of the different amino acids in the active site are also confirmed. The tyrosine residues are both found to be involved in substrate binding. Asp333 performs a nucleophilic attack on the epoxide, resulting in the formation of a covalent enzyme–substrate intermediate. This covalent intermediate is protonated by Tyr465. In our calculations, epoxide protonation occurs in a distinct step and not in concert with the alkylation step. His523 is found to act as a general base in the hydrolytic half-reaction, abstracting a proton from the catalytic water molecule. Asp495 is implicated in the charge-relay mechanism that facilitates water activation. A tetrahedral intermediate is observed during the hydrolytic half-reaction, which is stabilized by the oxyanion hole that is composed of hydrogen bonds from the backbone nitrogen atoms of Phe265 and Trp334. In the second step of the hydrolytic half-reaction, the protonated

His523 residue acts as a general acid and donates a proton to the alcohol oxygen atom of the Asp333 ester. This occurs in concert with cleavage of the ester bond, resulting in the formation of the vicinal diol.

The regioselectivity of epoxide attack was also addressed in our study. It has been shown that for (1*S*,2*S*)-β-methylstyrene oxide (MSO), attack at the benzylic position (C1) is preferred by 3.2 kcal mol^{-1}, indicating exclusive attack at this carbon center. The regioselectivity remains basically the same (3.6 kcal mol^{-1}) if the orientation of the MSO substrate is reversed. For (*S*)-styrene oxide (SSO), the calculated barriers for attack at the benzylic position (C1) and at the terminal carbon atom (C2) only differ by 0.7 kcal mol^{-1}, indicating that a mixture of products is formed. The results obtained show good agreement with experimentally determined regioselectivities for rodent-sEH-mediated hydrolysis of MSO and SSO.

Acknowledgements

We gratefully acknowledge financial help from The Swedish Research Council, The Wenner-Gren Foundations, The Carl Trygger Foundation, and The Magn Bergvall Foundation.

[1] A. J. Fretland, C. J. Omiecinski, *Chem.-Biol. Interact.* **2000**, *129*, 41–59.
[2] L. T. Laughlin, H.-F. Tzeng, S. Lin, R. N. Armstrong, *Biochemistry* **1998**, *37*, 2897–2904.
[3] M. Arand, H. Wagner, F. Oesch, *J. Biol. Chem.* **1996**, *271*, 4223–4229.
[4] F. Pinot, D. F. Grant, J. K. Beetham, A. G. Parker, B. Borhan, S. Landt, A. D. Jones, B. D. Hammock, *J. Biol. Chem.* **1995**, *270*, 7968–7974.
[5] R. Rink, F. Fennema, M. Smids, U. Dehmel, D. B. Janssen, *J. Biol. Chem.* **1997**, *272*, 14650–14657.
[6] H.-F. Tzeng, L. T. Laughlin, R. N. Armstrong, *Biochemistry* **1998**, *37*, 2905–2911.
[7] P. A. Bell, C. B. Kasper, *J. Biol. Chem.* **1993**, *268*, 14011–14017.
[8] J. W. Newman, C. Morisseau, B. D. Hammock, *Prog. Lipid Res.* **2005**, *44*, 1–51.
[9] R. N. Armstrong, C. S. Cassidy, *Drug Metab. Rev.* **2000**, *32*, 327–338.
[10] G. M. Lacourciere, R. N. Armstrong, *Chem. Res. Toxicol.* **1994**, *7*, 121–124.
[11] E. Blée, S. Summerer, M. Flenet, H. Rogniaux, A. van Dorsselaer, F. J. Schuber, *Biol. Chem.* **2005**, *280*, 6479–6487.
[12] L. T. Elfström, M. Widersten, *Biochem. J.* **2005**, *390*, 633–640.
[13] M. Arand, H. Hemmer, H. Dürk, J. Baratti, A. Archelas, R. Furstoss, F. Oesch, *Biochem. J.* **1999**, *344*, 273–280.
[14] J. Zou, B. M. Hallberg, T. Bergfors, F. Oesch, M. Arand, S. L. Mowbray, T. A. Jones, *Structure* **2000**, *8*, 111–122.
[15] H. Wojtasek, G. D. Prestwich, *Biochem. Biophys. Res. Commun.* **1996**, *220*, 323–329.
[16] E. J. de Vries, D. B. Janssen, *Curr. Opin. Biotechnol.* **2003**, *14*, 414–420.
[17] A. Steinreiber, K. Faber, *Curr. Opin. Biotechnol.* **2001**, *12*, 552–558.
[18] M. Arand, D. F. Grant, J. K. Beetham, T. Friedberg, F. Oesch, B. D. Hammock, *FEBS Lett.* **1994**, *338*, 251–256.
[19] B. Borhan, A. D. Jones, F. Pinot, D. F. Grant, M. J. Kurth, B. D. Hammock, *J. Biol. Chem.* **1995**, *270*, 26923–26930.
[20] F. Müller, M. Arand, H. Frank, A. Seidel, W. Hinz, L. Winkler, K. Hänel, E. Blée, J. K. Beetham, B. D. Hammock, F. Oesch, *Eur. J. Biochem.* **1997**, *245*, 490–496.
[21] B. D. Hammock, F. Pinot, J. K. Beetham, D. F. Grant, M. E. Arand, F. Oesch, *Biochem. Biophys. Res. Commun.* **1994**, *3*, 850–856.
[22] G. M. Lacourciere, R. N. Armstrong, *J. Am. Chem. Soc.* **1993**, *115*, 10466–10467.
[23] T. E. Creighton, *Proteins: Structures and Molecular Properties*, 2nd ed., Freeman, New York, **1993**.
[24] M. Nardini, I. S. Ridder, H. J. Rozeboom, K. H. Kalk, R. Rink, D. B. Janssen, B. W. Dijkstra, *J. Biol. Chem.* **1999**, *274*, 14579–14586.
[25] M. A. Argiriadi, C. Morisseau, B. D. Hammock, D. W. Christianson, *Proc. Natl. Acad. Sci. USA* **1999**, *96*, 10637–10642.
[26] M. A. Argiriadi, C. Morisseau, M. H. Goodrow, D. L. Dowdy, B. D. Hammock, D. W. Christianson, *J. Biol. Chem.* **2000**, *275*, 15265–15270.
[27] G. A. Gomez, C. Morisseau, B. D. Hammock, D. W. Christianson, *Biochemistry* **2004**, *43*, 4716–4723.
[28] R. Rink, J. Kingma, J. H. Lutje Spelberg, D. B. Janssen, *Biochemistry* **2000**, *39*, 5600–5613.
[29] T. Yamada, C. Morisseau, J. E. Maxwell, M. A. Argiriadi, D. W. Christianson, B. D. Hammock, *J. Biol. Chem.* **2000**, *275*, 23082–23088.
[30] S. M. Franken, H. J. Rozeboom, K. H. Kalk, B. W. Dijkstra, *EMBO J.* **1991**, *10*, 1297–1302.
[31] E. Y. Lau, Z. E. Newby, T. C. Bruice, *J. Am. Chem. Soc.* **2001**, *123*, 3350–3357.
[32] B. Schiøtt, T. C. Bruice, *J. Am. Chem. Soc.* **2002**, *124*, 14558–14570.
[33] a) C. Lee, W. Yang, R. G. Parr, *Phys. Rev. B* **1988**, *37*, 785–789; b) A. D. Becke, *Phys. Rev. A* **1988**, *38*, 3098–3100; c) A. D. Becke, *J. Chem. Phys.* **1992**, *96*, 2155–2160; d) A. D. Becke, *J. Chem. Phys.* **1992**, *97*, 9173–9177; e) A. D. Becke, *J. Chem. Phys.* **1993**, *98*, 5648–5652.
[34] Gaussian 03 (Revision A.1), M. J. Frisch, G. W. Trucks, H. B. Schlegel, G. E. Scuseria, M. A. Robb, J. R. Cheeseman, J. A. Montgomery, Jr., T. Vreven, K. N. Kudin, J. C. Burant, J. M. Millam, S. S. Iyengar, J. Tomasi, V. Barone, B. Mennucci, M. Cossi, G. Scalmani, N. Rega, G. A. Petersson, H. Nakatsuji, M. Hada, M. Ehara, K. Toyota, R. Fukuda, J. Hasegawa, M. Ishida, T. Nakajima, Y. Honda, O. Kitao, H. Nakai, M. Klene, X. Li, J. E. Knox, H. P. Hratchian, J. B. Cross, C. Adamo, J. Jaramillo, R. Gomperts, R. E. Stratmann, O. Yazyev, A. J. Austin, R. Cammi, C. Pomelli, J. W. Ochterski, P. Y. Ayala, K. Morokuma, G. A. Voth, P. Salvador, J. J. Dannenberg, V. G. Zakrzewski, S. Dapprich, A. D. Daniels, M. C. Strain, O. Farkas, D. K. Malick, A. D. Rabuck, K. Raghavachari, J. B. Foresman, J. V. Ortiz, Q. Cui, A. G. Baboul, S. Clifford, J. Cioslowski, B. B. Stefanov, G. Liu, A. Liashenko, P. Piskorz, I. Komaromi, R. L. Martin, D. J. Fox, T. Keith, M. A. Al-Laham, C. Y. Peng, A. Nanayakkara, M. Challacombe, P. M. W. Gill, B. Johnson, W. Chen, M. W. Wong, C. Gonzalez, J. A. Pople, Gaussian, Inc., Pittsburgh, PA, **2004**.
[35] a) A. Klamt, G. Schüürmann, *J. Chem. Soc., Perkin. Trans. 2* **1993**, 799–805; b) J. Andzelm, C. Kölmel, A. Klamt, *J. Chem. Phys.* **1995**, *103*, 9312–9320; c) V. Barone, M. Cossi, *J. Phys. Chem. A* **1998**, *102*, 1995–2001; d) M. Cossi, N. Rega, G. Scalmani, V. J. Barone, *Comput. Chem.* **2003**, *24*, 669–681.
[36] K. C. Williamson, C. Morisseau, J. E. Maxwell, B. D. Hammock, *Tetrahedron: Asymmetry* **2000**, *11*, 4451–4462.
[37] J. Baker, M. Muir, J. Andzelm, *J. Chem. Phys.* **1995**, *102*, 2063–2079.
[38] M. N. Glukhovtsev, R. D. Bach, A. Pross, L. Radom, *Chem. Phys. Lett.* **1996**, *260*, 558–564.
[39] B. G. Johnson, C. A. Gonzales, P. M. W. Gill, J. A. Pople, *Chem. Phys. Lett.* **1994**, *221*, 100–108.
[40] J. Clayden, N. Greeves, S. Warren, P. Wothers, *Organic Chemistry*, Oxford University Press Inc., New York, **2001**.
[41] H.-F. Tzeng, L. T. Laughlin, S. Lin, R. N. Armstrong, *J. Am. Chem. Soc.* **1996**, *118*, 9436–9437.
[42] R. Rink, D. B. Janssen, *Biochemistry* **1998**, *37*, 18119–18127.
[43] C. Morriseau, G. Du, J. W. Newman, B. D. Hammock, *Arch. Biochem. Biophys.* **1998**, *356*, 214–228.
[44] L. T. Elfström, M. Widersten, *Biochemistry* **2006**, *45*, 205–212.
[45] T. Ishida, S. Kato, *J. Am. Chem. Soc.* **2004**, *126*, 7111–7118.

[46] C.-H. Hu, T. Brinck, K. Hult, *Int. J. Quantum Chem.* **1998**, *69*, 89–103.
[47] G. Bellucci, C. Chiappe, A. Cordoni, F. Marioni, *Tetrahedron Lett.* **1994**, *35*, 4219–4222.
[48] P. Moussou, A. Archelas, J. Baratti, R. Furstoss, *Tetrahedron: Asymmetry* **1998**, *9*, 1539–1547.
[49] J. H. Lutje Spelberg, R. Rink, R. M. Kellogg, D. B. Janssen, *Tetrahedron: Asymmetry* **1998**, *9*, 459–466.

Received: December 5, 2005
Revised: March 28, 2006
Published online: July 20, 2006

